

Film transitions of receding contact lines

J. Ziegler, J.H. Snoeijer, and J. Eggers

School of Mathematics, University of Bristol, University Walk, Bristol BS8 1TW, United Kingdom

Abstract. When a solid plate is withdrawn from a liquid bath, a receding contact line is formed where solid, liquid, and gas meet. Above a critical speed U_{cr} , a stationary contact line can no longer exist and the solid will eventually be covered completely by a liquid film. Here we show that the bifurcation diagram of this coating transition changes qualitatively, from discontinuous to continuous, when decreasing the inclination angle θ_p of the plate. We show that this effect is governed by the presence of capillary waves, illustrating that the large scale flow strongly effects the maximum speed of dewetting.

The distinction between a dry solid and a solid covered by a liquid film is central for all painting and coating processes. In a system driven either by external motion of the solid or by gravity, this distinction is determined not only by the equilibrium properties of contact lines, but crucially by non-equilibrium solutions of moving contact lines. As a prototypical problem, consider a solid plate partially submerged in a liquid, which does not wet the solid. At rest, the fluid will form a static meniscus terminating at an angle corresponding to the equilibrium contact angle θ_e . A classical calculation due to Laplace [1,2] shows that the contact line rises (or falls) to a position of z relative to the equilibrium level of the bath:

$$z = \pm \ell_c \sqrt{2[1 - \cos(\theta_p - \theta_e)]}, \quad (1)$$

where θ_p is the plate inclination, $\ell_c = \sqrt{\gamma/(\rho g)}$ is the capillary length, and γ, ρ the surface tension and the density of the liquid, respectively. The \pm sign depends on whether θ_e is smaller (+) or larger (-) than the plate inclination.

If the plate is withdrawn from the liquid at a constant speed U , viscous forces will draw up the liquid, and the contact line position rises to a new, non-equilibrium value (cf. Fig. 1). This value results from the competition between viscous and capillary forces, so a proper dimensionless measure of U is the capillary number $Ca = \eta U / \gamma$, where η is the viscosity of the fluid. Above a critical value Ca_{cr} of the capillary number (typically $Ca_{cr} \lesssim 0.01$), a stationary contact line position is no longer sustainable, and in the long-time limit the plate is covered by a liquid film. According to classical phenomenological ideas [3], this transition occurs when the apparent contact angle, as observed macroscopically, goes to zero. From (1) this transition would thus occur as the contact line position reaches its maximal height $z_0 = \ell_c \sqrt{2(1 - \cos \theta_p)}$, which is $\approx \ell_c \theta_p$ for small θ_p .

This idea has recently been confirmed using asymptotic matching between the static solution (1) and the local fluid motion near the contact line [4,5]. The local motion is characterised by a microscopic length λ , which regularises the viscous stress singularity predicted by the Navier-Stokes equation. For $\lambda = 0$, no contact line motion would be possible [6]. The physical origin of λ may depend on the physical system at hand, but in this paper we are going to assume that the cut-off is due to fluid slip [7,8]. Typical values for λ are a few nanometres [9].

However, in principle there is a smaller speed Ca^* which is sufficient to initiate the entrainment of a liquid film. Snoeijer et al. [10,11] have investigated the intermediate situation

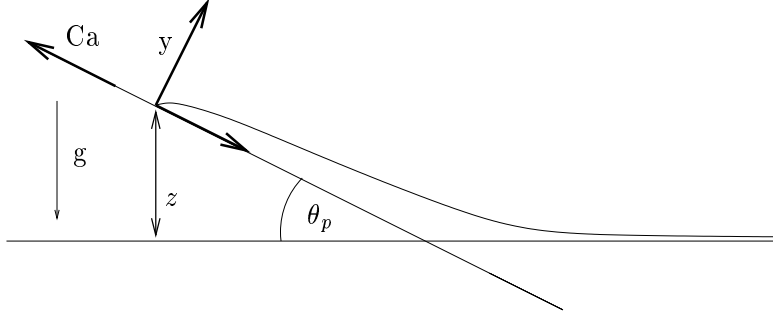


Fig. 1. A solid plate is withdrawn at constant speed from a bath of partially wetting liquid. The position of the meniscus is measured by z , the elevation over the bath.

of a liquid film that covers a partially dry substrate, and thus ends at a receding contact line. In the limit that the film is very long, its properties must become independent of the liquid meniscus, and the tip moves at a speed Ca^* that only depends on the static contact angle θ_e and the slip length λ . Thus, if the plate speed is greater than Ca^* , a film can be entrained, given appropriate initial conditions.

In this paper we investigate the bifurcation diagram of the entrainment transition as function of the plate angle θ_p . This comes about since Ca_{cr} and Ca^* have a different dependence on the inclination of the plate. Above a critical value of θ_p^{cr} , $Ca_{cr} > Ca^*$, and the transition towards the coating layer is discontinuous. Namely, once the speed is raised (slightly) above Ca_{cr} , the contact line moves up at a *finite* speed $Ca_{cr} - Ca^*$. At θ_p^{cr} , however, Ca_{cr} drops below Ca^* and the film develops as soon as the plate speed is greater than Ca^* . In this case the speed at which the contact line moves up becomes arbitrarily small at threshold. Another striking feature is that for small inclinations the maximum height of the meniscus no longer obeys the 'zero contact angle' argument predicting a finite z_0 at the transition. We show that the critical height becomes much larger than predicted by (1) and even diverges below a critical plate inclination.

Results. We numerically solved for the shapes of stationary menisci, characterised by the liquid thickness $h(x)$, using the lubrication approximation [12,13]. This long wavelength expansion remains quantitatively accurate when the interface slope remains small, $h' \ll 1$, so we consider small plate inclinations only. As the equilibrium contact angle enters as a boundary condition $h' = \theta_e$ at the contact line, it is convenient to use the rescaled height $\bar{h} = h/\theta_e$, such that $\bar{h}' = 1$. If we further introduce $\bar{\theta} = \theta_p/\theta_e$, $\bar{\lambda} = \lambda/\theta_e$ and $\delta = 3Ca/\theta_e^3$, and dropping overbars, the equation for the meniscus becomes [4]:

$$h''' - h' + \theta = \frac{\delta}{h^2 + 3\lambda^2}. \quad (2)$$

All lengths are expressed in the capillary length ℓ_c , typically a millimetre, while we take the slip-length $\lambda = 3.3 \times 10^{-3}$ throughout the paper.¹ The boundary conditions for this third order equation are thus $h = 0$ and $h' = 1$ at the contact line, and the third condition comes from matching to the bath, $h \simeq x\theta$ as $x \rightarrow \infty$. Solutions are found numerically using a shooting procedure.

The results are conveniently represented in terms of the meniscus elevation z , see Fig. 2 (a). For moderate plate inclination ($\theta = 1$), z increases with the (rescaled) plate velocity δ , until a saddle-node bifurcation occurs at δ_{cr} . The elevation curve then undergoes an infinite

¹ This convenient slip law slightly differs from the usual Navier slip condition, as the latter yields a diverging h''' at the contact line. This choice has been shown to have no effect on the macroscopic physics [4].

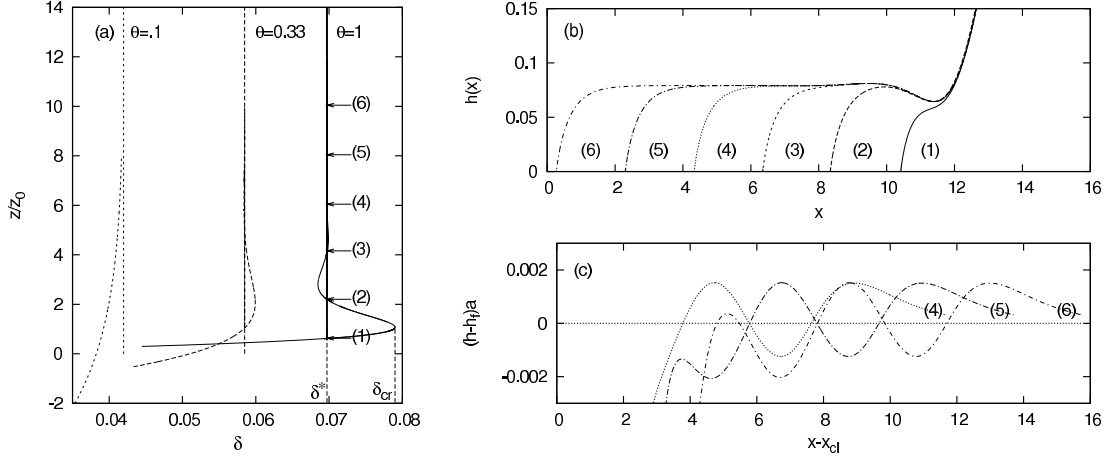


Fig. 2. (a) Bifurcation diagrams: meniscus rise z vs. plate speed δ for various plate inclinations θ . At a critical θ^{cr} the difference between $\delta_{cr} - \delta^*$ vanishes and the transition becomes continuous. (b) Meniscus profiles $h(x)$ for $\theta = 1.0$ at locations separated by $\ell_{osc}/2$. (c) To visualise capillary waves on the film, which are exponentially damped, we multiplied $(h - h_f)$ by a factor $a = 10^{-0.5(x-x_{cl})}$, where x_{cl} is the position of the contact line. The solutions (4) and (6) are exactly in phase, whereas (5) is shifted by half a wavelength.

series of exponentially damped oscillations around another critical speed δ^* , each corresponding to a saddle-node bifurcation. The oscillations are seen to have a well-defined wavelength ℓ_{osc} . Profiles corresponding to the marked arrows are shown in panel (b), revealing increasingly long films of almost uniform thickness $h_f = \sqrt{\delta^*/\theta}$ as one moves up the elevation curve. The natural speed of a film, ending in a contact line, is δ^* . As the plate velocity is raised above δ_{cr} , a front will start to move up the plate at a *finite* speed $\delta_{cr} - \delta^*$. However, another scenario observed experimentally [10] is a jump to the film solution as soon as δ^* is reached. The reason for this discontinuous behaviour is not understood at present.

As the plate inclination decreases, the oscillations on the elevation curve become smaller (cf. Fig. 2 (a)), and have vanished entirely for $\theta = 0.1$, making the transition toward a film continuous. We now show that the oscillations in the bifurcation diagram are directly related to small ripples on the actual profiles seen in Fig. 2 (b), and which have the *same wavelength* ℓ_{wave} , as seen in the expanded scale, panel (c). As one moves up the elevation curve by $\ell_{osc}/2$, one additional half-wave fits onto the profile, causing successive profiles in panel (b) to line up exactly, confirming that $\ell_{osc} = \ell_{wave}$. One observes that solutions for which δ is at a local maximum (minimum), the oscillation has positive (negative) amplitude close to the contact line. This is consistent with the fact that dissipation is stronger when the thickness is thinner.

The above observations imply that the oscillations in the bifurcation diagram can be understood completely in terms of (small) oscillations around a liquid film, obtained by linearising (2) around h_f . The wavelength ℓ_{wave} is easily found to be

$$\ell_{wave} = \begin{cases} 4\pi / (r^{-1/3} - r^{1/3}) & \text{if } \alpha \geq 1 \\ \infty & \text{if } \alpha \leq 1 \end{cases}, \quad (3)$$

where $\alpha = \frac{27\theta^3}{\delta^*}$ and $r = \sqrt{\alpha} - \sqrt{\alpha - 1}$. Perfect agreement between the analytical result (3) and ℓ_{osc} as measured from the bifurcation diagrams is seen in Fig. 3 (a) for various plate inclinations θ . At a critical value $\theta^{cr} = (\delta^*/27)^{1/3} = 0.108$ the wavelength diverges and oscillations disappear altogether. The numerical value will weakly depend on the slip length λ . At the same inclination, at which the film transition becomes continuous, the elevation z_{cr} at the entrainment transition diverges. To further test our analytical criterion for this change of behaviour, we plotted the speeds δ_{cr} and δ^* as function of θ (cf. Fig. 3 (b)). Indeed, at $\theta = \theta_{cr}$, the two speeds become identical and the “bump” seen in Fig. 2 (a) goes away.

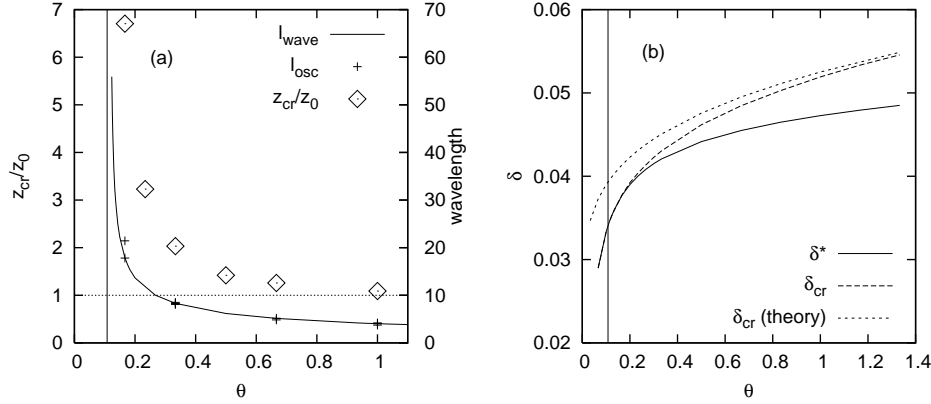


Fig. 3. (a) Right axis: the wavelength ℓ_{osc} (+) compared to ℓ_{wave} (solid line), as computed from (3). Left axis: comparison of the elevation at the wetting transition, z_{cr} , to the prediction of zero apparent contact angle, z_0 (\diamond). The ratio z_{cr}/z_0 diverges as θ_{cr} is approached. (b) Dependence of δ_{cr} (dashed line) and δ^* (solid line) on the plate inclination θ . The short-dashed line is the theoretical prediction from asymptotic matching [4,5], which breaks down for small inclinations.

Outlook. We have shown that the transition towards liquid deposition can be continuous or discontinuous, depending on the inclination of the plate. This provides a striking demonstration of the fact that maximum speed of dewetting is not an intrinsic property of the contact line, as has been claimed in an earlier paper [14], but subtly depends on the large scale geometry of the problem. A very similar analysis applies to the shape of two-dimensional drops or ridges sliding down an inclined plane [15]. Their shapes had previously been found numerically, and used as a model problem to study the stability of contact lines [16,17]. At high speeds (large volumes) sliding drops acquire a long tail, which correspond to the film solutions seen in Fig. 2 (b). This contrasts the behaviour of real three-dimensional drops [18,19], which eventually eject a small rivulet out of their rear.

References

1. P. S. de Laplace, *Mechanique Celeste Supplement au X Livre*, (Courier, Paris 1805).
2. L. D. Landau and E. M. Lifshitz, *Fluid Mechanics*, (Pergamon, Oxford 1984).
3. B. V. Deryagin and S. M. Levi, *Film Coating Theory* (Focal, London 1964).
4. J. Eggers, Phys. Rev. Lett. **93**, 094502 (2004).
5. J. Eggers, Phys. Fluids **17**, 082106, (2005).
6. C. Huh and L. E. Scriven, J. Coll. Int. Sci. **35**, 85 (1971).
7. L. M. Hocking, Q. J. Appl. Math. **36**, 55 (1983).
8. T. Qian, X.-P. Wang and P. Sheng, J. Fluid Mech. **564**, 333 (2006).
9. C. Cottin-Bizonne, B. Cross, A. Steinberger and E. Charlaix, Phys. Rev. Lett. **94**, 056102 (2005).
10. J. H. Snoeijer, G. Delon, M. Fermigier and B. Andreotti, Phys. Rev. Lett. **96**, 174504 (2006).
11. J. H. Snoeijer, B. Andreotti, G. Delon and M. Fermigier, J. Fluid Mech. **579**, 63 (2007).
12. A. Oron, S. H. Davis and S. G. Bankoff, Rev. Mod. Phys. **69**, 931 (1997).
13. L. M. Hocking, Euro. J. Appl. Math. **12**, 195 (2001).
14. P. G. de Gennes, Coll. Pol. Sci. **264**, 463 (1986).
15. J. Ziegler, J. H. Snoeijer and J. Eggers, in preparation.
16. U. Thiele and E. Knobloch, Phys. Fluids **15**, 892 (2003).
17. L. Kondic, SIAM Review **45**, 95 (2003).
18. T. Podgorski, J. M. Flesselles and L. Limat, Phys. Rev. Lett. **87**, 036102 (2001).
19. J. H. Snoeijer, N. Le Grand Piteira, L. Limat, H. A. Stone and J. Eggers, Phys. Fluids **19**, 042104 (2007).